Geomechanics and Engineering, *Vol. 22, No. 4 (2020) 291-303*
DOI: https://doi.org/10.12989/gae.2020.22.4.291

Probabilistic analysis of tunnel collapse: Bayesian method for detecting change points

Binghua Zhou, Yiguo Xue*, Shucai Li, Daohong Qiu, Yufan Tao, Kai Zhang, Xueliang Zhang and Teng Xia

Geotechnical and Structural Engineering Research Center, Shandong University, Ji'nan 250061, Shandong, China

(Received January 6, 2019, Revised May 18, 2020, Accepted July 9, 2020)

Abstract. The deformation of the rock surrounding a tunnel manifests due to the stress redistribution within the surrounding rock. By observing the deformation of the surrounding rock, we can not only determine the stability of the surrounding rock and supporting structure but also predict the future state of the surrounding rock. In this paper, we used grey system theory to analyse the factors that affect the deformation of the rock surrounding a tunnel. The results show that the 5 main influencing factors are longitudinal wave velocity, tunnel burial depth, groundwater development, surrounding rock support type and construction management level. Furthermore, we used seismic prospecting data, preliminary survey data and excavated section monitoring data to establish a neural network learning model to predict the total amount of deformation of the surrounding rock during tunnel collapse. Subsequently, the probability of a change in deformation in each predicted section was obtained by using a Bayesian method for detecting change points. Finally, through an analysis of the distribution of the change probability and a comparison with the actual situation, we deduced the survey mark at which collapse would most likely occur. Surface collapse suddenly occurred when the tunnel was excavated to this predicted distance. This work further proved that the Bayesian method can accurately detect change points for risk evaluation, enhancing the accuracy of tunnel collapse forecasting. This research provides a reference and a guide for future research on the probability analysis of tunnel collapse.

Keywords: tunnel collapse; deformation prediction; Bayesian method; detecting change points

1. Introduction

A tunnel is an engineering body that exists under complex geological conditions. The complex geological environment present and various construction techniques used determine the complexity of the mechanical properties of the surrounding rock. The deformation of the rock surrounding a tunnel manifests due to the stress redistribution within the surrounding rock. By observing the deformation of the surrounding rock, we can not only determine the stability of the surrounding rock and supporting structure but also predict the future state of the surrounding rock. When the deformation of surrounding rock exceeds a certain threshold, it will destroy the initial support and may even cause the surrounding rock to collapse. Tunnel collapse will cause casualties and considerable economic losses. Therefore, predicting the stability of surrounding rock is of great significance to risk assessment.

Duan *et al.* (2016) described the failure mechanism of a rock mass in true triaxial tests based on three-dimensional DEM simulations. Yagiz (2011) tested nine rock materials by thin section analysis to establish empirical equations for the longitudinal wave velocity and rock dynamic parameters to predict the rock characteristics. Senent *et al.* (2013) determined the critical collapse pressure of a rock mass based on the Hoek-Brown nonlinear failure criterion. Huang *et al.* (2017) derived an analytical expression of the collapse surface from variational calculation in the framework of the upper bound theorem. Su *et al.* (2010) established the general expression for the limit state equation of the stability of the surrounding rock. In the abovementioned work, the failure mechanism of a rock mass was studied by means of experimental and numerical simulations, which laid a theoretical foundation for the study of the stability of the rock surrounding a tunnel.

Pan *et al.* (2016) used kinematics and numerical simulations to study the effect of pore water pressure on tunnel face stability. The effects of weathering parameters and pore water on initial block collapse are described in two- and three-dimensional analyses by Qin and Chian. (2017). The results of Li *et al.* (2016) show that the sequential excavation method can promote face stability and reduce ground displacement during tunnel excavation. The condition of the unexcavated rock can be obtained through advanced detection methods. Jetschny *et al.* (2010) studied the influence of the propagation characteristics of tunnel surface waves in a rock mass by advanced seismic detection. Gong *et al.* (2010) proposed a combined migration velocity analysis and imaging method based on Kirchhoff integral migration and reverse time migration to predict the geological structure of a tunnel. The abovementioned achievements are mainly from studies that focused on a single factor to evaluate the status and stability of rock surrounding a tunnel. It is well known that the instability of rock surrounding a tunnel is the result of multiple factors. With the development of nonlinear

*Corresponding author, Professor, Ph.D.
E-mail: xieagle@sdu.edu.cn

ISSN: 2005-307X (Print), 2092-6219 (Online)

disciplines (Liu *et al.* 2017, Zhou *et al.* 2015, Cevik *et al.* 2011), increasingly more scholars have evaluated the stability of surrounding rock by combining various influencing factors by using nonlinear theory. Xue and Xiao (2017) proposed the PSO-LSSVM model to predict the deformation of the surrounding rock during ground excavation. Ocak and Seker (2013) focused on surface settlement prediction using three different methods: artificial neural networks, support vector machines, and Gaussian processes. Rezaei *et al.* (2015) used two predictive methods, namely, a Mamdani fuzzy system and multivariable regression analysis, to predict the deformation modulus of surrounding rock. To control deformation during construction, the degree of influence of multiple factors on the tunnel deformation is analysed by data mining, and a deformation prediction model was established by Xue *et al.* (2018). Li *et al.* (2015) analysed the sensitivity of tunnel stability factors by using the grey correlation method and analysing quantitative data. Ma and Fu (2014) achieved a realistic stability analysis of a rock mass with a proposed probabilistic rock mass model. Tian *et al.* (2016) developed Bayesian approaches for probabilistic characterization of the inherent spatial variability of the effective friction angle of sand in a statistically homogenous sand layer. Wang *et al.* (2017a) established a Bayesian network collapse prediction model to assess the risk of tunnel collapse. Gong *et al.* (2008) presented a method to forecast the over-excavation of ground opening projects by using Bayes discriminant analysis theory. Yuan *et al.* (2016) established a tunnel collapse risk assessment model based on catastrophe theory through a quantitative analysis and multi-index criteria. Wang *et al.* (2017b) used normal cloud model theory to create a multi-index evaluation model for rockfall risk assessment. Alimoradi *et al.* (2008) used a trained artificial neural network to estimate the unknown nonlinear relationships from the results of tunnel seismic prediction and those obtained by rock mass rating classification. Shi *et al.* (2014) proposed an advanced optimized classification method to accurately predict the classification of the surrounding rock based on a fuzzy analytic hierarchy process and tunnel seismic prediction. The risk of mountain tunnel collapse was used by Zhang *et al.* (2015) as an example to illustrate a new assessment method based on case-based reasoning, advanced geological prediction, and rough set theory.

At present, nonlinear evaluation methods have been widely used in tunnel engineering and have achieved good results. However, the abovementioned achievements do not include combining the nonlinear method with Bayesian probability to analyse tunnel collapse data and detect change points. In addition, unlike the previous tunnel collapse prediction models, the method presented in this paper predicts the deformation of the rock surrounding the excavation face by utilizing grey relational analysis and artificial neural networks. In addition, based on the deformation of the surrounding rock, a Bayesian method for detecting change points is used to obtain the locations of possible landslides and to guide on-site construction decisions. This study first describes the actual deformation of the studied tunnel, then analyses the influencing factors based on the actual engineering sample, and finally determines a deformation prediction of the location of the change in deformation. This work enhances the accuracy of tunnel collapse forecasting and provides a bridge between fundamental development and practical application. This research provided a reference and a guide for future research on the probability analysis of tunnel collapse.

2. Methodology

2.1 Grey system theory

Grey relational analysis is a system analysis method that combines qualitative and quantitative approaches to distinguish the relationship between systems, as described by the grey relational degree obtained from the quantitative method (Yeh and Chen 2004, Zhang *et al.* 2018). In the process of system development, if the variation trend of two factors is consistent, that is, if the degree of synchronous change is high, the degree of correlation is considered to be high. In contrast, if the degree of synchronous change is low, the degree of correlation is low. The steps to evaluate the factors affecting the deformation of rock surrounding a tunnel by grey correlation are as follows:

Step 1. The evaluation index system is determined. We use the factors influencing the deformation of the rock surrounding a tunnel as the original evaluation matrix and take the deformation of the rock surrounding a tunnel as the reference series.

It is assumed that the evaluation problem contains m objects and n indicators. The original evaluation matrix is Eq. (1).

$$\mathrm{X} = \begin{bmatrix} X_1 \\ X_2 \\ \cdots \\ X_i \\ \cdots \\ X_m \end{bmatrix} = \begin{bmatrix} x_{11} & \cdots & x_{1n} \\ \vdots & \ddots & \vdots \\ x_{m1} & \cdots & x_{mn} \end{bmatrix} \tag{1}$$

where x_{ig} represents the index value of the gth index of the ith object.

According to the influencing factors of the surrounding rock deformation, the reference sequence of the surrounding rock deformation is set to $X_0 = (x_{01}, x_{02} \cdots x_{0n})$.

Step 2. The index data are normalized, and the data sequence after normalization is recorded as Eq. (2).

$$Z = \begin{bmatrix} Z_0 \\ Z_1 \\ \cdots \\ Z_i \\ \cdots \\ Z_m \end{bmatrix} = \begin{bmatrix} z_{01} & \cdots & z_{0n} \\ z_{11} & \cdots & z_{1n} \\ \vdots & \ddots & \vdots \\ z_{m1} & \cdots & z_{mn} \end{bmatrix} \tag{2}$$

where $Z_0 = (z_{01}, z_{02} \cdots z_{0n})$ is the normalized reference sequence.

Step 3. For the standardized data sequence, we calculate the absolute difference between the index of the influencing factors of the surrounding rock deformation and the corresponding element of the sequence of the surrounding rock deformation, one by one, i.e.,

$$\left|Z_i - Z_0\right| = \left|z_{ij} - z_{0j}\right| \left(i = 1, 2, \cdots, m, j = 1, 2, \cdots, n\right) \tag{3}$$

Step 4. $\min\limits_{i=1}^{m}\left\{\min\limits_{j=1}^{m}\left(\left|z_{ij} - z_{0j}\right|\right)\right\}$ and $\max\limits_{i=1}^{m}\left\{\max\limits_{j=1}^{m}\left(\left|z_{ij} - z_{0j}\right|\right)\right\}$ are determined.

Step 5. Eq. (4) is used to calculate the incidence coefficient between the index of the influencing factors of the surrounding rock deformation and the corresponding element of the sequence of the surrounding rock deformation.

$$\zeta_{ij} = \frac{\min\limits_{i=1}^{m}\left\{\min\limits_{i=1}^{n}\left(\left|z_{ij} - z_{0j}\right|\right)\right\} + \eta \cdot \max\limits_{i=1}^{m}\left\{\max\limits_{i=1}^{n}\left(\left|z_{ij} - z_{0j}\right|\right)\right\}}{\left|z_{ij} - z_{0j}\right| + \eta \cdot \max\limits_{i=1}^{m}\left\{\max\limits_{i=1}^{n}\left(\left|z_{ij} - z_{0j}\right|\right)\right\}} \tag{4}$$

where η is the resolution coefficient and is between 0 and 1. The lower the value of η is, the greater the difference between the resolution coefficients and the stronger the resolution ability. In general, $\eta = 0.5$ is assumed. The correlation coefficient ζ_{ij} is a positive number less than or equal to 1 and reflects the degree of correlation between the ith influence factor of the index sequence X_i of the surrounding rock deformation and the jth attribute of the deformation sequence X_0 of the surrounding rock.

Step 6. The correlation degree is calculated.

We calculate the average of the correlation coefficients between the influencing factors of the surrounding rock deformation and corresponding elements of the surrounding rock deformation sequence, following Eq. (5).

$$P = \left(p_{01}, p_{02}, \cdots, p_{0m}\right)^T \tag{5}$$

where $p_{0i} = \frac{1}{n}\sum\limits_{j=1}^{n}\xi_{ij}\left(j\right), i = 1, 2, \cdots, m, j = 1, 2, \cdots, n$.

Step 7. According to the correlation degree of the influencing factors of the deformation of the rock surrounding a tunnel, we obtain comprehensive evaluation results.

2.2 Artificial neural network model

A back-propagation neural network (Fig. 1) is a feedback-type, fully connected multilayer neural network with strong associative memory and generalization ability (Funahashi 1989; Specht 1990). Here, $D = \left\{\left(x_1, y_1\right), \left(x_2, y_2\right), \cdots \left(x_m, y_m\right)\right\}, x_m \in R^d, y_m \in R^l$ is given, where x_m is the mth input value of the input layer of factors influencing the deformation of the surrounding rock. R^d indicates that the input rock deformation factors are described by d attributes. R^l is an output one-dimensional real-valued vector of vault subsidence and horizontal convergence. The process of neural network training for the deformation of the surrounding rock is expressed as follows.

Step 1. The loss function is determined.

For the sample $\left(x_k, y_k\right)$, we assume that the output of the neural network is $\hat{y}_k = \left(\hat{y}_1^k, \hat{y}_2^k \cdots, \hat{y}_l^k\right)$, i.e.,

$$\hat{y}_k = f\left(\beta_j - \theta_j\right) \tag{6}$$

where θ_j is the threshold of the jth neuron in the output layer.

The mean squared error of the neural network in the sample is given by Eq. (7).

$$E_k = \frac{1}{2}\sum_{j=1}^{l}\left(\hat{y}_j^k - y_j^k\right)^2 \tag{7}$$

Step 2. The parameter adjustment strategy is defined. The neural network is based on a gradient descent strategy and adjusts the parameters in the negative gradient direction of the target.

$$\begin{aligned} v &= v + \Delta v \\ \Delta v &= -\eta \frac{\partial E_k}{\partial v} \end{aligned} \tag{8}$$

Step 3. The gradient $\frac{\partial E_k}{\partial v}$ of the output layer threshold θ_j is calculated.

$\hat{y}_j^k$ has a direct impact on E_k, and θ_j has a direct impact on $\hat{y}_j^k$. Therefore, we can obtain Eq. (9) by the chain rule.

$$\frac{\partial E_k}{\partial \theta_j} = \frac{\partial E_k}{\partial \hat{y}_j^k} \cdot \frac{\partial \hat{y}_j^k}{\partial \theta_j} \tag{9}$$

We can obtain Eq. (10) from Eq. (7).

$$\frac{\partial E_k}{\partial \hat{y}_j^k} = \hat{y}_j^k - y_j^k \tag{10}$$

The activation function is a sigmoid function, and we can obtain Eq. (11) from Eq. (6).

$$\frac{\partial \hat{y}_j^k}{\partial \theta_j} = -\hat{y}_j^k\left(1 - \hat{y}_j^k\right) \tag{11}$$

$$\frac{\partial E_k}{\partial \theta_j} = \frac{\partial E_k}{\partial \hat{y}_j^k} \cdot \frac{\partial \hat{y}_j^k}{\partial \theta_j} = \hat{y}_j^k\left(1 - \hat{y}_j^k\right)\left(y_j^k - \hat{y}_j^k\right) \tag{12}$$

Eq. (12) is written as Eq. (13).

$$g_j = \frac{\partial E_k}{\partial \theta_j} = \hat{y}_j^k\left(1 - \hat{y}_j^k\right)\left(y_j^k - \hat{y}_j^k\right) \tag{13}$$

Step 4. The ratio $\frac{\partial E^k}{\partial w_{hj}}$ of the hidden layer to the output layer connection weight w_{hj} is calculated. $\hat{y}_j^k$ has a direct impact on E_k, β_j has a direct impact on $\hat{y}_j^k$, and

w_{hj} has a direct impact on β_j. Therefore, we can obtain Eq. (9) by the chain rule.

$$\frac{\partial E_k}{\partial w_{hj}} = \frac{\partial E_k}{\partial \hat{y}_j^k} \cdot \frac{\partial \hat{y}_j^k}{\partial \beta_j} \cdot \frac{\partial \beta_j}{\partial w_{hj}} \tag{14}$$

where w_{hj} is the connection weight of the hth and jth neurons in the hidden layer, β_j is the input of the jth neuron in the output layer, and b_h is the hth neuron output of the hidden layer.

$\frac{\partial \beta_j}{\partial w_{hj}} = b_h$ since $\frac{\partial \hat{y}_j^k}{\partial \beta_j} = \hat{y}_j^k \left(1 - \hat{y}_j^k\right)$

We can obtain Eq. (15) from Eq. (13).

$$\frac{\partial E_k}{\partial w_{hj}} = -g_j \cdot b_h \tag{15}$$

Step 5. The gradient $\frac{\partial E^k}{\partial \gamma_h}$ of the hidden layer threshold γ_h is calculated.

b_h has a direct impact on E_k, and γ_h has a direct impact on b_h. Therefore, we can obtain Eq. (11) by the chain rule.

$$\frac{\partial E_k}{\partial \gamma_h} = \frac{\partial E_k}{\partial b_h} \cdot \frac{\partial b_h}{\partial \gamma_h} \tag{16}$$

where γ_h is the hth neuron threshold of the hidden layer.

$$\sum_{j=1}^{l} \frac{\partial E_k}{\partial \hat{y}_j^k} \cdot \frac{\partial \hat{y}_j^k}{\partial \beta_j} \cdot \frac{\partial \beta_j}{\partial b_h} = -\sum_{j=1}^{l} g_j w_{hj} \tag{17}$$

$$\frac{\partial b_h}{\partial \gamma_h} = \frac{\partial}{\partial \gamma_h} f\left(a_h - \gamma_h\right) = -f'\left(a_h - \gamma_h\right) = -b_h\left(1 - b_h\right) \tag{18}$$

We can obtain Eq. (19) from Eq. (17) and Eq. (18).

$$\frac{\partial E_k}{\partial \gamma_h} = b_h\left(1 - b_h\right) \sum_{j=1}^{l} g_j w_{hj} \tag{19}$$

Step 6. The inductive conclusions are drawn.

In the multilayer forward network, the threshold gradient $g_h^{(m)}$ of the hidden layer is expressed as the threshold gradient of the m-layer. The hidden-layer neuron output is expressed as the output of $b_h^{(m)}$ the m-layer neurons. The connection weight of the hidden layer and the output layer is expressed as the weight $w_{hj}^{(m+1)}$ of the m+1-layer. The threshold gradient $g_j^{(m+1)}$ of the output layer is expressed as the threshold gradient of the m-layer. Then, Eq. (19) changes into Eq. (20).

$$g_h^m = b_h^m\left(1 - b_h^m\right) \sum_{j=1}^{l} w_{hj}^{(m+1)} g_j^{(m+1)} \tag{20}$$

The connection weight gradient $\frac{\partial E^k}{\partial w_{hj}}$ of the hidden layer and the output layer is expressed as the m-layer connection weight gradient $\frac{\partial E^k}{\partial w_{hj}}$. g_j is expressed as the m-layer threshold gradient $g_j^{(m)}$. b_h is expressed as the m-1 layer output $b_h^{(m-1)}$. Then, Eq. (15) changes into Eq. (21).

$$p_{hj}^{(m)} = -g_j^{(m)} b_h^{(m-1)} \tag{21}$$

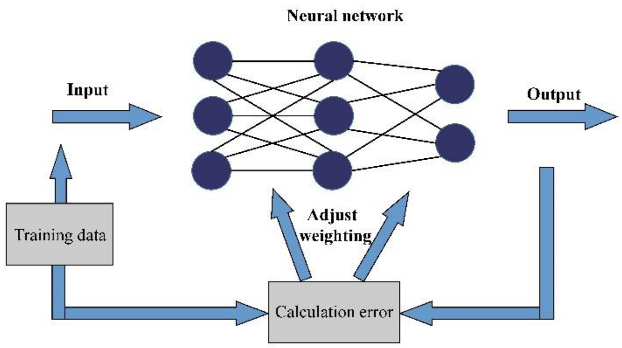

Fig. 1 Schematic diagram of a three-layer neural network

Combining Eq. (20) and Eq. (21), we can calculate the threshold gradient of the current layer of neurons and the gradient of the connection weight if we know the threshold gradient of the neurons in the previous layer. According to Eq. (13), we can calculate the threshold gradient of the neurons in the output layer, so the neural threshold and the gradient of the connection weight can also be calculated. This work can create the training network.

2.3 Bayesian method for detecting change points

Change points are determined by an instantaneous change in the statistical characteristic of a sequence or process. This change often reflects a qualitative change. The key point of the Bayesian method of point analysis is to treat the parameters in the model as random variables, introducing a probability distribution called the prior distribution. We use the prior distribution and the sample distribution to determine the posterior distribution of the variable point. In addition, we introduce a necessary inference based on the posterior distribution (Barry and Hartigan 1993, Perreault *et al.* 2000).

According to the law of large numbers, we assume that the spatial sequence of observations concerning the deformation of rock surrounding a tunnel obeys a normal distribution. If the factors influencing the spatial sequence of the deformation of rock surrounding a tunnel abruptly change at a point, the statistical parameters that belong to observation Z_i of the normal distribution will no longer be the same on both sides of the point. Before the change point, the distribution density function of observation Z_i is Eq. (22). After the change point, the distribution density function of observation Z_i is Eq. (23).

$$Z_i \sim N\left\{\mu_1, \sigma_1^2\right\}\left(i = 1, 2, \wedge, j\right) \tag{22}$$

$$Z_i \sim N\left\{\mu_2, \sigma_2^2\right\}\left(i = j+1, \wedge, n\right) \tag{23}$$

where μ_1 is the expected value of j before the change point, μ_2 is the expected value of j after the change point, σ_1^2 is the variance in j before the change point, and σ_2^2 is the variance in j after the change point.

When determining whether the mean value of the spatial sequence of the deformation of the rock surrounding a tunnel changes, we assume a constant variance, i.e.,

$$\sigma_1^2 = \sigma_2^2 = \sigma^2 \tag{24}$$

where the value of σ^2 can be estimated from the observations of the spatial sequence of surrounding rock deformation. In addition, we assume that μ_1 and μ_2 obey the same normal distribution, i.e.,

$$\mu_1 \sim N\left(\mu_0, \sigma_0^2\right) \tag{25}$$

$$\mu_2 \sim N\left(\mu_0, \sigma_0^2\right) \tag{26}$$

According to the Bayesian theorem, we can deduce the posterior probability distribution from the distribution parameters μ_1 and μ_2 after obtaining the spatial sequence of the deformation of the rock surrounding a tunnel, $Z = \left(Z_i, Z^{j+1}\right)$.

The posterior distribution of μ_1 derived from the observation information Z_j is Eq. (27).

$$\mu_1 / Z_j \sim N\left(\mu_1, \sigma_1^2\right) \tag{27}$$

where $\mu_1 = \dfrac{\left(n\mu_1 + \sum_{i=1}^{j} Z_i\right)}{(n+j)}$, $\sigma_1^2 = \dfrac{\sigma^2}{(n+j)}$, and $n = \dfrac{\sigma^2}{\sigma_0^2}$.

The posterior distribution of μ_2 derived from the observation information Z_{j+1} is Eq. (28).

$$\mu_2 / Z_{j+1} \sim N\left(\mu_2, \sigma_2^2\right) \tag{28}$$

where $\mu_2 = \dfrac{\left(n\mu_2 + \sum_{i=j+1}^{n} Z_i\right)}{n+(n-j)}$, $\sigma_2^2 = \dfrac{\sigma^2}{n+(n-j)}$, and $n = \dfrac{\sigma^2}{\sigma_0^2}$.

The posterior distribution density function for the change point is deduced in two steps:

Step 1. The joint distribution function of the observed data is Eq. (29) when μ_1 and μ_2 are known.

$$p\left(Z/_j, \mu_1, \mu_2\right) = \prod_{i=1}^{j} \frac{1}{\sigma\sqrt{2\pi}} exp\left[-\frac{(Z_i - \mu_1)}{2\sigma^2}\right] \cdot \prod_{i=j+1}^{n} \frac{1}{\sigma\sqrt{2\pi}} exp\left[-\frac{(Z_i - \mu_2)}{2\sigma^2}\right] \tag{29}$$

Step 2. According to the Bayesian principle, the posterior distribution density function for deducing the position of the change point is Eq. (30).

$$p\left(j/_Z, \mu_1, \mu_2\right) = \frac{p\left(Z/_j, \mu_1, \mu_2\right) p(j)}{\sum_{i=1}^{n} p\left(Z/_i, \mu_1, \mu_2\right) p(i)} \tag{30}$$

2.4 The seismic prospecting method

Seismic prospecting is an advanced technology for predicting the geological condition ahead of the tunnel excavation face and is an artificial seismic exploration method that uses seismic reflection waves. When a seismic incident wave meets stratigraphic interfaces and structural surfaces, especially fault fracture zones, karst caves, underground rivers and other undesirable geological interfaces, reflected waves that can be received by a receiver and output by a digital recorder will be produce. The spreading velocity, delay time, waveform, intensity, and direction of the reflected wave are related to the nature and appearance of the relevant interface, which is represented by different types of data and used to predict the presence of adverse geologic bodies in front of the face (Li *et al.* 2017).

3. Project overview

The Longtan tunnel is one of the important control projects along the Hurongxi highway between Yichang and Enshi. The length of the left tunnel is 8694 m, while the length of the right tunnel is 8620 m. In addition, the maximum burial depth of the Longtan tunnel is 530 m. As shown in Fig. 2, the tunnel is located in an area with an eroded valley landscape, a geomorphology that has extreme topographical conditions. The Longtan tunnel is known by experts as a "Geological Museum" and "Geological Disaster Encyclopedia".

The rocks in the study area mainly represent two types of lithology. One is weakly weathered sandy shale and argillaceous sandstone, which is distributed along ZK65+516~ZK70+420 in the left tunnel and YK65+520~YK70+880 in the right tunnel. The other is weakly weathered limestone and dolomite, which is distributed along ZK70+420~ZK74+200 in the left tunnel and YK70+880~YK74+200 in the right tunnel. There are two faults in the tunnel area: F1 and F2. The strike of F1 is NW, and its inclination direction is to the NE. The strike of F2 is NW, and its inclination direction is to E. Some karst has developed in the area of the Longtan tunnel.

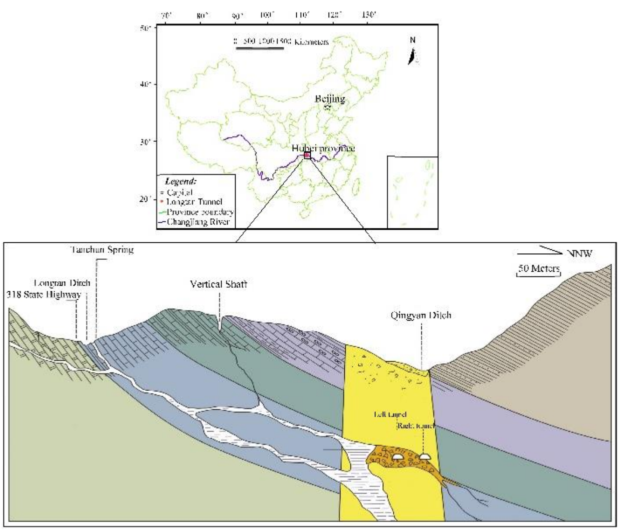

Fig. 2 Schematic diagram of the Longtan tunnel (Xue *et al.* 2008)

4. Analysis of factors affecting tunnel deformation

4.1 The influence factors of tunnel deformation

The influence factors of the deformation of the rock surrounding a tunnel are numerous and complex. It is difficult to analyse each factor when assessing the deformation of the rock surrounding a tunnel. Therefore, we choose several of the major influential factors. In this paper, according to the actual deformation of the surrounding rock in the Longtan tunnel and other tunnel engineering cases, we selected eight important factors as indicators for evaluating the deformation characteristics of rock surrounding a tunnel, as shown in Table 1: longitudinal wave velocity, density, Poisson's ratio, tunnel burial depth, groundwater development, surrounding rock support type, support close time and construction management level.

(1) Longitudinal wave velocity (A1)

The strength and integrity of the surrounding rock have a great influence on its stability. In the detection of seismic waves, the longitudinal wave velocity is a direct response to the strength and integrity of the surrounding rock. This index value can be determined using seismic wave detection.

(2) Density (A2)

Rock excavation is an unloading process. Excavation unloading will cause the original cracks to open or new fractures to form, resulting in a change in the density of the rock mass. Excavation unloading will affect the stability of the surrounding rock, and its index value can be determined using seismic wave detection.

(3) Poisson's ratio (A3)

Poisson's ratio is the absolute value of the ratio of the transverse strain to the longitudinal strain caused by an evenly distributed longitudinal stress. Poisson's ratio is also an important physical quantity that can characterize the deformation properties of a rock mass, and its index value can be determined using seismic wave detection.

(4) Tunnel burial depth (A4)

A tunnel will lose its natural arch shape as the burial depth of the tunnel decreases. The influence of excavation will spread to the surface, impeding the formation of natural arches, and the surrounding rock will lose its ability to self-stabilize. In general, the stability of the surrounding rock will worsen as the burial depth of the tunnel becomes shallower. This index value can be obtained from previously gathered survey data.

(5) Groundwater development (A5)

Groundwater is an important factor affecting the stability of the surrounding rock. The role of water is mainly manifested in the corrosion of the rocks and the erosion of the filling material. Groundwater will soften the rocks and reduce their strength. This index value can be determined using seismic wave detection. Groundwater development deduced from seismic waves is a qualitative indicator, but we can quantify it by using Table 2.

(6) Surrounding rock support type (A6)

When the tunnel is excavated, the stress of the rock mass is released, causing deformation and collapse. Therefore, effective control of the surrounding rock is the key to ensuring the initial stability of the surrounding rock. The radial stress provided by the initial support greatly improves the stress state of the rock around the tunnel. The data of the excavated section can be obtained based on the site engineering data, and the data of the unexcavated section can be obtained based on the design data. The quantitative standards are shown in Table 3.

(7) Support close time (A7)

Close time is the time required to excavate from the surface to the initial support sealing ring. An early support close time has an important effect on the stability of a tunnel because the plastic zone quickly develops after unloading of the surrounding rock. The surrounding rock pressure and deformation will increase greatly once loose damage occurs, threatening the stability of the rock surrounding a tunnel. These indicators can be obtained according to field engineering data.

(8) Construction management level (A8)

Engineering disturbance directly causes collapse, and factors such as improper excavation methods are directly related to tunnel collapse. The construction factors are

Table 1 Influencing factors of the deformation of rock surrounding a tunnel

Serial number	Influencing factors	Serial number	Influencing factors
A1	Longitudinal wave velocity (m/s)	A5	Groundwater development
A2	Density (kg/ m^3)	A6	Surrounding rock support type
A3	Poisson's ratio	A7	Support close time (d)
A4	Burial depth of tunnel (m)	A8	Construction management level

Table 2 Grade division of groundwater

Grade division	Specific description	Parameter value
I	The groundwater is very well developed and causes a major problem. The results of the interpretation show that the reflection energy of the S wave is stronger than that of the P wave, the S wave manifests as reflective stripe bandwidth with good extensibility, and the V_p/V_s increases considerably.	0-0.2
II	The groundwater is developed, and it presents a moderate water pressure. The results of the interpretation show that the S wave reflection energy is clearly stronger than the P wave, and the V_p/V_s suddenly increases.	0.2-0.5
III	The groundwater is quite developed, and there is a small amount of fissure water. The results of the interpretation show that the S wave reflection energy is stronger than the P wave reflection energy.	0.5-0.8
IV	Groundwater is not developed, and the rock is dry. There is no water-bearing feature in the interpretation results.	0.8-1.0

Table 3 Quantization table of support type

Support type	Parameter value	Support type	Parameter value
S2-a	1	S3	4
S2-1	2	S4	5
S2-2	3	S5	6

Table 4 Grade division of construction management level

Grade division	Specific description	Parameter value
I	Construction experience and technical ability are extremely insufficient.	0-0.2
II	Construction experience and technical ability are poor.	0.2-0.4
III	Construction experience and technical ability are fair.	0.4-0.6
IV	Construction experience and technical ability are good.	0.6-0.8
V	Construction experience and technical ability are superior.	0.8-1.0

Table 5 Evaluation samples of factors affecting the surrounding rock deformation

	A1 (m/s)	A2 (kg/m^3)	A3	A4 (m)	A5	A6	A7 (d)	A8	B1 (mm)	B2 (mm)
1	2892	2.16	0.25	413	0.9	3	16	0.7	-19.6	-7.6
2	1996	2.19	0.21	260	0.7	1	17	0.7	-42.4	-25.2
3	2876	2.15	0.21	381	0.8	2	16	0.7	-19.5	-9.8
4	2291	2.53	0.2	312	0.6	2	17	0.9	-31.8	-17.3
5	2330	2.12	0.24	299	0.6	2	18	0.9	-32.1	-16.7
6	2954	2.21	0.19	372	0.9	3	17	0.7	-18.2	-8.9
7	1778	2.43	0.2	291	0.6	3	15	0.9	-45.9	-26.1
8	1510	2.39	0.23	266	0.7	2	16	0.7	-38.7	-22.3
9	2976	2.15	0.26	391	0.8	2	18	0.9	-23.2	-13.5
10	2943	2.15	0.24	354	0.8	3	16	0.9	-23.9	-14.2
11	2422	2.16	0.2	269	0.9	3	16	0.7	-31.2	-15.9
12	2959	2.19	0.28	336	0.9	2	15	0.9	-28.6	-12.1
13	2115	2.31	0.25	336	0.7	2	16	0.9	-33.7	-25.3
14	2276	2.24	0.24	376	0.9	3	16	0.7	-22.1	-8.9
15	2643	2.01	0.19	411	0.8	3	15	0.9	-23.9	-16.6
16	2933	2.43	0.19	392	0.9	2	14	0.9	-25.2	-16.1
17	2969	2.24	0.24	361	0.8	2	13	0.7	-20.9	-10.8
18	2976	2.19	0.29	402	0.9	2	15	0.7	-18.5	-11.4
19	2931	2.23	0.24	360	0.9	2	15	0.7	-19.2	-10.7
20	2902	2.19	0.17	291	0.8	3	14	0.9	-28.5	-18.2
21	2989	2.27	0.24	302	0.7	3	14	0.9	-30.9	-21.6
22	2973	2.35	0.22	394	0.9	3	15	0.7	-22.4	-10.4
23	2945	2.12	0.23	286	0.6	3	15	0.9	-39.5	-21.5
24	3105	2.18	0.25	310	0.9	4	13	0.9	-21.1	-10.6
25	3367	2.25	0.23	382	0.8	4	15	0.7	-20.6	-12.1

constrained by the quality of the construction unit of the project. To simplify the analysis, the technology and management levels of the construction unit are categorized according to Table 4.

4.2 Evaluation index of tunnel deformation

(1) Vault subsidence (B1)

This index reflects the vertical settlement of a tunnel. Due to the engineering nature of a rock mass, vertical settlement is usually caused by underfoot sinking, and it mainly occurs before the initial support closure. Vault subsidence is an important basis for determining the stability of a tunnel during construction.

(2) Horizontal convergence (B2)

This index reflects the horizontal deformation of the tunnel cross section. This deformation is usually caused by the deformation of the arch frame, and its value will affect the overall shape and stress distribution of the arch, which has an important influence on the engineering quality and construction safety. Horizontal deformation will cause longitudinal cracking of the initial support and may even lead to tunnel collapse if the horizontal convergence is too large.

Table 6 Analysis results of the attribute correlation

	A1	A2	A3	A4	A5	A6	A7	A8
B1	0.040	0.024	0.025	0.037	0.031	0.040	0.022	0.033
B2	0.034	0.030	0.031	0.046	0.042	0.034	0.028	0.045

4.3 Reduction factor

The effects of different indexes on the deformation of the Longtan tunnel vary. Some of these factors may be selected for redundancy. We determine the main factors that affect the deformation and construct the optimal property set, which can reasonably predict the deformation of the Longtan tunnel. As shown in Table 5, numerous monitoring data of excavated sections are selected, and a model evaluation sample is constructed. Then, we use grey relational grade evaluation theory to calculate the correlation degree of the surrounding rock deformation to different deformation factors.

According to Eq. (3), the correlation degree of vault subsidence is calculated for each deformation factor after establishing the evaluation sample of factors affecting the surrounding rock deformation. Similarly, this work is also completed for horizontal convergence.

As shown in Table 6, the influence of each index on vault subsidence and horizontal convergence are analysed, and the correlation degree between these factors is compared. We find that the main influencing factors were A1, A4, A5, A6 and A8. Among these five factors, some reflect the geological aspects of the Longtan tunnel, while others are construction-related factors. These indicators are also the main controlling factors of the deformation of the Longtan tunnel.

5. Prediction of the deformation of the rock surrounding a tunnel

5.1 Constructing neural network learning samples

The sample of a neural network must be representative and uniform; therefore, a learning sample set was constructed, as shown in Table 7. There are five neurons in the input layer: longitudinal wave velocity, tunnel burial depth, groundwater development, surrounding rock support type and construction management level. The output layer

Table 7 Neural network learning samples of surrounding rock deformation

	Input					Output	
	A1 (m/s)	A4 (m)	A5	A6	A8	B1 (mm)	B2 (mm)
1	2892	413	0.9	3	0.7	-19.6	-7.6
2	1996	260	0.7	1	0.7	-42.4	-25.2
3	2876	381	0.8	2	0.7	-19.5	-9.8
4	2291	312	0.6	2	0.9	-31.8	-17.3
5	2330	299	0.6	2	0.9	-32.1	-16.7
6	2954	372	0.9	3	0.7	-18.2	-8.9
7	1778	291	0.6	3	0.9	-45.9	-26.1
8	1510	266	0.7	2	0.7	-38.7	-22.3
9	2976	391	0.8	2	0.9	-23.2	-13.5
10	2943	354	0.8	3	0.9	-23.9	-14.2
11	2422	269	0.9	3	0.7	-31.2	-15.9
12	2959	336	0.9	2	0.9	-28.6	-12.1
13	2115	336	0.7	2	0.9	-33.7	-25.3
14	2276	376	0.9	3	0.7	-22.1	-8.9
15	2643	411	0.8	3	0.9	-23.9	-16.6
16	2933	392	0.9	2	0.9	-25.2	-16.1
17	2969	361	0.8	2	0.7	-20.9	-10.8
18	2976	402	0.9	2	0.7	-18.5	-11.4
19	2931	360	0.9	2	0.7	-19.2	-10.7
20	2902	291	0.8	3	0.9	-28.5	-18.2
21	2989	302	0.7	3	0.9	-30.9	-21.6
22	2973	394	0.9	3	0.7	-22.4	-10.4
23	2945	286	0.6	3	0.9	-39.5	-21.5
24	3105	310	0.9	4	0.9	-21.1	-10.6
25	3367	382	0.8	4	0.7	-20.6	-12.1

Table 8 Optimal neural network model information

Number of input neurons	Number of output neurons	Number of hidden layers	Number of neurons in the hidden layer	Target error	Epochs	Learning accuracy
5	2	1	11	0.05	10000	0.01

utilized two neurons: vault subsidence and horizontal convergence.

5.2 Neural network input model

After obtaining the sample set, the raw input and output data were converted into valid numeric data. The input vector X was obtained from the longitudinal wave velocity, tunnel burial depth, groundwater development, surrounding rock support type and construction management level. The output vector Y was obtained from the vault subsidence and horizontal convergence. As shown in Table 8, an implicit layer was created. After repeated debugging, the convergence of the network improved when the number of nodes in the hidden layer was 11 and the learning accuracy was 0.01; this information can be used for inversion calculation. Additionally, each sample is input into the network for learning, and the mean squared error of the output stabilized after 10000 iterations. The MATLAB training error curve is shown in Fig. 3(a), and the correlation coefficient of the optimal neural network model is shown in Fig. 3(b).

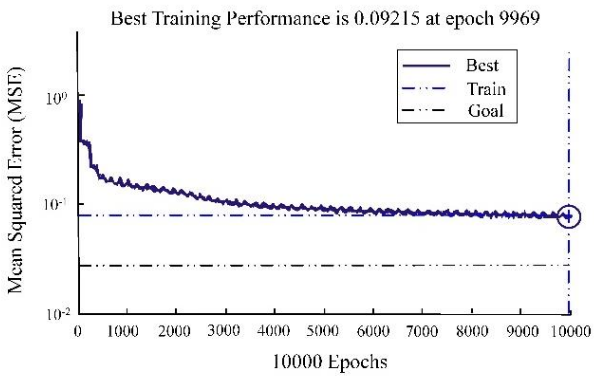

(a) Training error curve

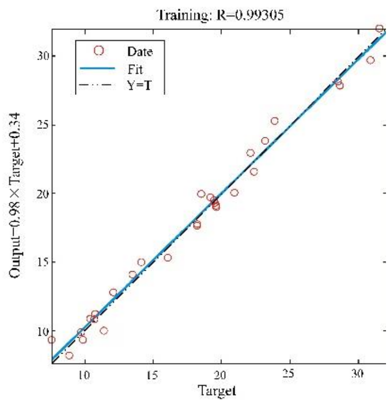

(b) Correlation coefficient of model

Fig. 3 Neural network learning

Table 9 Input parameters of the neural network model

Survey mark	A1 (m/s)	A4 (m)	A5	A6	A8
ZK72+200	2921	320	0.4	4	0.9
ZK72+190	2920	320	0.3	4	0.7
ZK72+180	2921	320	0.3	4	0.9
ZK72+170	2921	324	0.4	4	0.7
ZK72+160	3003	324	0.8	4	0.9
ZK72+150	3003	326	0.8	4	0.7
ZK72+140	3003	324	0.8	4	0.9
ZK72+130	3003	324	0.8	4	0.7
ZK72+120	3025	320	0.8	4	0.9
ZK72+110	3087	320	0.8	4	0.7

5.3 Prediction of surrounding rock deformation

The neural network model established above was used with the valid input parameters presented in Table 9. As shown in Table 10, the vault subsidence and horizontal convergence were obtained for the Longtan tunnel from ZK72+200 to ZK72+110.

Table 10 Prediction table of vault subsidence and horizontal convergence

	ZK72+200	ZK72+190	ZK72+180	ZK72+170	ZK72+160	ZK72+150	ZK72+140	ZK72+130	ZK72+120	ZK72+110
Vault Subsidence (mm)	-46.66	-39.11	-41.25	-42.04	-37.45	-38.87	-35.45	-39.12	-33.66	-39.20
Horizontal convergence (mm)	-28.09	-20.44	-21.94	-23.51	-22.46	-24.16	-22.46	-24.27	-22.54	-24.33

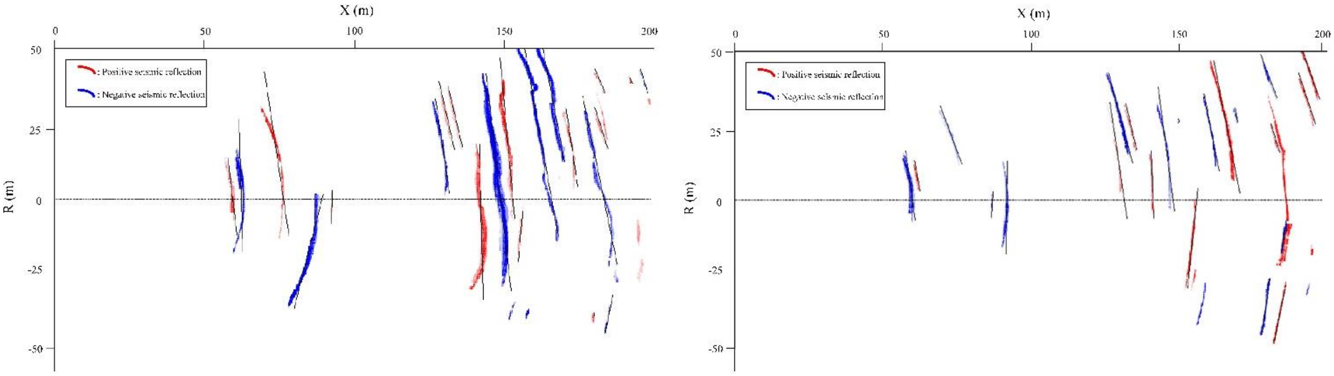

(a) P waves (b) SH waves

Fig. 4 Depth migration diagram (Xue *et al.* 2008)

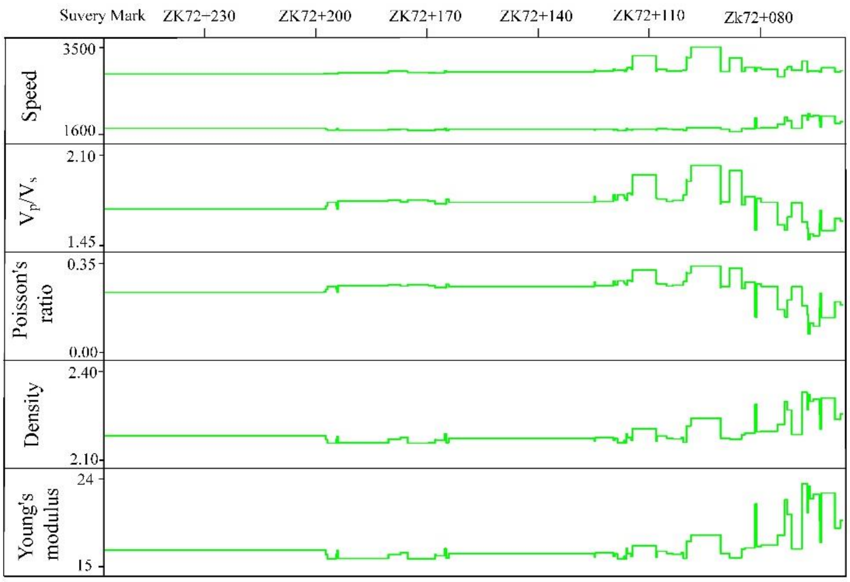

Fig. 5 Diagram of the physical properties (Xue *et al.* 2008)

6. Engineering field evaluation

6.1 Advanced forecast

In the previous engineering geological exploration work of the Longtan tunnel, the geological engineering was complex at ZK72+200~ZK72+110; here, tunnel collapse is more likely. Therefore, we applied the seismic prospecting method to detect the surrounding rocks at ZK72+204. The results of the seismic wave detection and interpretation are shown in Figs. 4 and 5.

According to the detection results (Figs. 4 and 5) at ZK72+200~ ZK72+160, as the seismic shear wave decreases, the longitudinal wave increases slightly, the VP/VS ratio increases, Poisson's ratio suddenly increases, and the density and Young's modulus decrease; therefore, there is a greater possibility of rock collapse in front of ZK72+204 due to the poor properties of the rock mass and the presence of fluids.

6.2 Detecting change points of surrounding rock deformation

Given various external forces, the tunnel structure will produce certain changes. These changes can usually be expressed by the amount of deformation. The most direct manifestation of tunnel collapse is indicated by the change points of the surrounding rock deformation. The posterior probability distribution of the potential collapse position in

Table 11 Posterior probability of change point occurrence

	ZK72+200	ZK72+190	ZK72+180	ZK72+170	ZK72+160	ZK72+150	ZK72+140	ZK72+130	ZK72+120	ZK72+110
Vault subsidence	0.029	0.029	0.029	0.329	0.188	0.283	0.029	0.029	0.029	0.029
Horizontal convergence	0.021	0.021	0.021	0.299	0.275	0.281	0.021	0.021	0.021	0.021

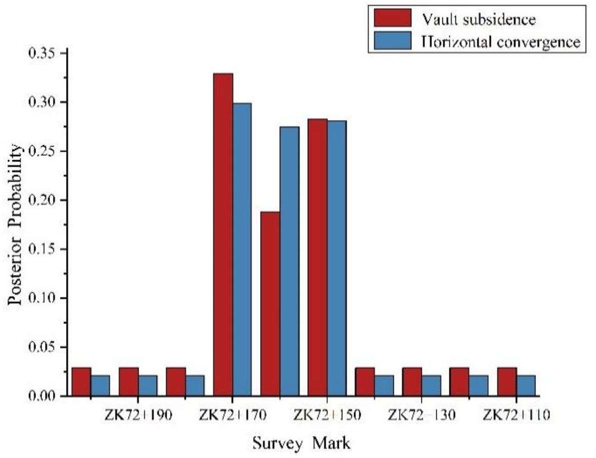

Fig. 6 Histogram of posterior probability distribution for change point location

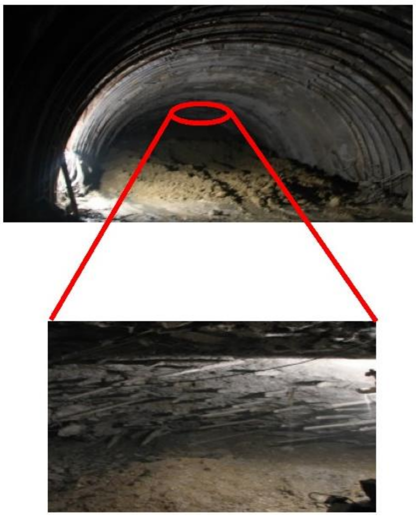

Fig. 7 A photograph of the tunnel collapse

the Longtan tunnel is obtained by using the Bayesian method for detecting change points based on the results of the seismic prospecting method and the prediction of the surrounding rock deformation. According to the probability distribution, we can precisely locate the future collapse position to guide the informatization of engineering construction.

We applied the Bayesian method for detecting change points to study the trend of the prediction data of vault subsidence and horizontal convergence along ZK72+200~ZK72+110 in the Longtan tunnel. The change points in each section were calculated by Eq. (14) and Eq. (15), as shown in Table 11. The location with the largest posterior probability is regarded as the location of the most likely change point.

Fig. 6 shows that the predicted values of vault subsidence and horizontal convergence denote an area with a higher probability of change point presence. At ZK72+170, the posterior probability of a change point in vault subsidence is 0.329, and the posterior probability of a change point in horizontal convergence is 0.299. At ZK72+160, the posterior probability of a change point in vault subsidence is 0.188, and the posterior probability of a change point in horizontal convergence is 0.275. At ZK72+150, the posterior probability of a change point in vault subsidence is 0.283, and the posterior probability of a change point in horizontal convergence is 0.281. Combined with the above results and site-specific conditions, it can be inferred that collapse is more likely to occur when the surface is excavated to ZK72+170~ZK72+150. However, at the time of construction, attention should be paid to the deformation of the surrounding rock, and an emergency plan should be made to ensure the safety of construction personnel.

6.3 Site-specific conditions

The surface collapsed (Fig. 7) when the tunnel was excavated to ZK72+167. In the collapsed section, the silty earth fillings were flow-shaped, as in a debris flow. The debris blocked the flow of water, allowing the water to penetrate the vault and side arch of the initial support. This process led to a substantial increase in the water content of the surrounding rock at the vault and side arch and reduced the cohesion in the surrounding rock. Therefore, the initial pressure greatly increased, resulting in the deformation, cracking, and collapse of the support system.

7. Discussion

The success of a neural network depends on the diversity of the training samples. When the training samples are diversified, the training accuracy is higher. In this paper, the deformation of the rock surrounding the Longtan tunnel is predicted by a neural network. The learning sample is the monitoring data of the previously excavated tunnel section, and the result is the total deformation under normal excavation. However, there are no actual monitoring data to describe the total deformation amount due to the collapse that occurred during tunnel excavation. In the future, via sharing resources, substantial data processing, and multidisciplinary cooperation, more comprehensive and reliable data on the deformation of the surrounding rock during tunnel collapse can be used, and the deformation prediction model can be redeveloped. This work provides a new method of practical and convenient batch processing with which researchers can address this problem.

The tunnel collapse evaluation model in this study exhibited high reliability in Longtan tunnel. However, tunnel collapse evaluation is a complex and comprehensive system. If the risk of tunnel collapse requires a higher comprehensive and accurate evaluation result, the relevant research must be improved. Initially, many factors exert certain impact on the deformation of the rock surrounding a tunnel, and the deformation mechanism is complex. It is necessary to analyze the deformation factors of different types of tunnels to offer a more effective reference for future research. For example, factor numbers related to collapsibility can be increased in loess tunnel. Then, it is crucial to identify and analyze the influencing factors of tunnel collapse. If multiple methods can be combined, the tunnel collapse risk comprehensive evaluation system will be more accurate and perfect. Moreover, the quantification of longitudinal wave velocity and groundwater development condition in this study was based on the detection accuracy of the seismic prospecting method. Only by improving the accuracy of this seismic prospecting method and data interpretation can the accuracy of the method be improved.

8. Conclusions

In this paper, we used the grey system theory to analyse 8 factors that affect the deformation of rock surrounding a tunnel. The results show that the 5 main influencing factors are longitudinal wave velocity, tunnel burial depth, groundwater development, surrounding rock support type and construction management level. Among these five factors, some reflect the geological aspects of the Longtan tunnel, while others are construction-related factors. These indicators are also the main controlling factors of the deformation of the Longtan tunnel.

We used tunnel monitoring data from the excavated section of the Longtan tunnel to establish a neural network model consisting of five input neurons, one hidden layer, 11 hidden layer neurons, and two output neurons. Furthermore, we used seismic prospecting data and preliminary survey data to predict the total amount of deformation of the rock surrounding a tunnel collapse.

The posterior probability distribution of the potential collapse position in the Longtan tunnel is obtained by using the Bayesian method for detecting change points based on the results of the seismic prospecting method and the prediction of the surrounding rock deformation. At ZK72+170, the posterior probability of a change point in vault subsidence is 0.329, and the posterior probability of a change point in horizontal convergence is 0.299. At ZK72+160, the posterior probability of a change point in vault subsidence is 0.188, and the posterior probability of a change point in horizontal convergence is 0.275. At ZK72+150, the posterior probability of a change point in vault subsidence is 0.283, and the posterior probability of a change point in horizontal convergence is 0.281. Considering the above-mentioned results and site-specific conditions, it can be inferred that collapse is most likely to occur when the surface is excavated to ZK72+170~ZK72+150; during construction, surface collapse suddenly occurred when the tunnel was excavated to this predicted distance. This research provides a reference and a guide for future research on the probability analysis of tunnel collapse.

Acknowledgments

Much of the work presented in this paper was supported by the National Natural Science Foundations of China (grant numbers 41877239, 51379112, 51422904 and 41772298), and the State Key Development Program for Basic Research of China (grant number 2013CB036002), and the Fundamental Research Funds of Shandong University (grant number 2018JC044), and Shandong Provincial Natural Science Foundation (grant number JQ201513). The authors would like to express appreciation to the reviewers for their valuable comments and suggestions that helped improve the quality of our paper.

References

Alimoradi, A., Moradzadeh, A., Naderi, R., Salehi, M.Z. and Etemadi, A. (2008), "Prediction of geological hazardous zones in front of a tunnel face using TSP-203 and artificial neural networks", *Tunn. Undergr. Sp. Technol.*, **23**(6), 711-717. https://doi.org/10.1016/j.tust.2008.01.001.

Barry, D. and Hartigan, J.A. (1993), "A Bayesian analysis for change point problems", *J. Am. Stat. Assoc.*, **88**(421), 309-319. https://doi.org/10.1080/01621459.1993.10594323.

Cevik, A., Sezer, E.A., Cabalar, A.F. and Gokceoglu, C. (2011), "Modeling of the uniaxial compressive strength of some clay-bearing rocks using neural network", *Appl. Soft Comput.*, **11**(2), 2587-2594. https://doi.org/10.1016/j.asoc.2010.10.008.

Duan, K., Kwok, C.Y. and Ma, X.D. (2016), "DEM simulations of sandstone under true triaxial compressive tests", *Acta Geotech.*, **12**(3), 495-510. https://doi.org/10.1007/s11440-016-0480-6.

Funahashi, K. (1989), "On the approximate realization of continuous mappings by neural networks", *Neural Networks*, **2**(3), 183-192. https://doi.org/10.1016/0893-6080(89)90003-8.

Gong, F.Q., Li, X.B. and Zhang, W. (2008), "Over-excavation forecast of ground opening by using Bayes discriminant analysis method", *J. Cent. South Univ. Technol.*, **15**(4), 498-502. https://doi.org/10.1007/s11771-008-0094-8.

Gong, X.B., Han, L.G., Niu, J.J., Zhang, X.P., Wang, D.L. and Du, L.Z. (2010), "Combined migration velocity model-building and its application in tunnel seismic prediction", *Appl. Geophys.*, **7**(3), 265-271. https://doi.org/10.1007/s11770-010-0251-3.

Huang, F., Zhao, L.H., Ling, T.H. and Yang, X.L. (2017), "Rock mass collapse mechanism of concealed karst cave beneath deep tunnel", *Int. J. Rock Mech. Min. Sci.*, **91**, 133-138. https://doi.org/10.1016/j.ijrmms.2016.11.017.

Jetschny, S., Bohlen, T. and De Nil, D. (2010), "On the propagation characteristics of tunnel surface-waves for seismic prediction", *Geophys. Prospec.*, **58**(2), 245-256. https://doi.org/10.1111/j.1365-2478.2009.00823.x.

Li, P.F., Zhao, Y. and Zhou, X.J. (2016), "Displacement characteristics of high-speed railway tunnel construction in loess ground by using multi-step excavation method", *Tunn. Undergr. Sp. Technol.*, **51**, 41-55. https://doi.org/10.1016/j.tust.2015.10.009.

Li, S.C., Liu, B., Xu, X.J., Nie, L.C., Liu, Z.Y., Song, J., Sun, H.F., Chen, L. and Fan, K.R. (2017), "An overview of ahead geological prospecting in tunneling", *Tunn. Undergr. Sp. Technol.*, **63**, 69-94. https://doi.org/10.1016/j.tust.2016.12.011.

Li, Y.Y., Zheng, Y.R. and Kang, N. (2015), "Sensitivity analysis on influencing factors of tunnel stability", *Chin. J. Undergr. Sp. Eng.*, **11**(2), 491-498.

Liu, Y.L., Huang, X.L., Duan, J. and Zhang, H.M. (2017), "The assessment of traffic accident risk based on grey relational analysis and fuzzy comprehensive evaluation method", *Nat. Hazards*, **88**(3), 1409-1422. https://doi.org/10.1007/s11069-017-2923-2.

Ma, G.W. and Fu, G.Y. (2014), "A rational and realistic rock mass modelling strategy for the stability analysis of blocky rock mass", *Geomech. Geoeng.*, **9**(2), 113-123. https://doi.org/10.1080/17486025.2013.871067.

Ocak, I. and Seker, S.E. (2013), "Calculation of surface settlements caused by EPBM tunneling using artificial neural network, SVM, and Gaussian processes", *Environ. Earth Sci.*, **70**(3), 1263-1276. https://doi.org/10.1007/s12665-012-2214-x.

Pan, Q.J. and Dias, D. (2016), "The effect of pore water pressure on tunnel face stability", *Int. J. Numer. Anal. Meth. Geomech.*, **40**(15), 2123-2136. https://doi.org/10.1002/nag.2528.

Perreault, L., Bernier, J., Bobee, B. and Parent, E. (2000), "Bayesian change-point analysis in hydrometeorological time series", *J. Hydrol.*, **235**(3-4), 221-241. https://doi.org/10.1016/S0022-1694(00)00270-5.

Qin, C.B. and Chian, S.C. (2017), "2D and 3D stability analysis of tunnel roof collapse in stratified rock: A kinematic approach", *Int. J. Rock Mech. Min. Sci.*, **100**, 269-277. https://doi.org/10.1016/j.ijrmms.2017.10.027.

Rezaei, M., Asadizadeh, M., Majdi, A. and Hossaini, M.F. (2015), "Prediction of representative deformation modulus of longwall panel roof rock strata using Mamdani fuzzy system", *Int. J. Min. Sci. Technol.*, **25**(1), 23-30. https://doi.org/10.1016/j.ijmst.2014.11.007.

Senent, S., Mollon, G. and Jimenez, R. (2013), "Tunnel face stability in heavily fractured rock masses that follow the Hoek-Brown failure criterion", *Int. J. Rock Mech. Min. Sci.*, **60**, 440-451. https://doi.org/10.1016/j.ijrmms.2013.01.004.

Shi, S.S., Li, S.C., Li, L.P., Zhou, Z.Q. and Wang, J. (2014), "Advance optimized classification and application of surrounding rock based on fuzzy analytic hierarchy process and Tunnel Seismic Prediction", *Automat. Constr.*, **37**(1), 217-222. https://doi.org/10.1016/j.autcon.2013.08.019.

Specht, D.F. (1990), "Probabilistic neural networks", *Neural Networks*, **3**(1), 109-118. https://doi.org/10.1016/0893-6080(90)90049-Q.

Su, Y.H., Li, X., Zhao, M.H. and Xie, Z.Y. (2010), "Failure probability calculation for surrounding rock stability of tunnel considering random parameter distribution characteristics", *Chin. J. Comput. Mech.*, **27**(1), 120-126.

Tian, M., Li, D.Q., Cao, Z.J., Phoon, K.K. and Wang, Y. (2016), "Bayesian identification of random field model using indirect test data", *Eng. Geol.*, **210**, 197-211. https://doi.org/10.1016/j.enggeo.2016.05.013.

Wang, J., Li, S.C., Li, L.P., Shi, S.S., Xu, Z.H. and Lin, P. (2017a), "Collapse risk evaluation method on Bayesian network prediction model and engineering application", *Adv. Comput. Des.*, **2**(2), 121-131. https://doi.org/10.12989/acd.2017.2.2.121.

Wang, X.T., Li, S.C., Ma, X.Y., Xue, Y.G., Hu, J. and Li, Z.Q. (2017b), "Risk assessment of rockfall hazards in a tunnel portal section based on normal cloud model", *Pol. J. Environ. Stud.*, **26**(5), 2295-2306. https://doi.org/10.15244/pjoes/68427.

Xue, X.H. and Xiao, M. (2017), "Deformation evaluation on surrounding rocks of ground caverns based on PSO-LSSVM", *Tunn. Undergr. Sp. Technol.*, **69**, 171-181. https://doi.org/10.1016/j.tust.2017.06.019.

Xue, Y.G., Li, S.C., Zhang, Q.S., Li., S.C., Su, M.X. and Liu, Q (2008), "Prediction and early-warning technology of geological hazards in tunnel informational construction", *J. Shandong Univ. Eng. Sci.*, **38**(5), 25-30.

Xue, Y.G., Zhang, X.L., Li, S.C., Qiu, D.H., Su, M.X., Li, L.P., Li, Z.Q. and Tao, Y.F. (2018), "Analysis of factors influencing tunnel deformation in loess deposits by data mining: A deformation prediction model", *Eng. Geol.*, **232**, 94-103. https://doi.org/10.1016/j.enggeo.2017.11.014.

Yagiz, S. (2011), "P-wave velocity test for assessment of geotechnical properties of some rock materials", *B. Mater. Sci.*, **34**(4), 947-953. https://doi.org/10.1007/s12034-011-0220-3.

Yeh, Y.L. and Chen, T.C. (2004), "Application of grey correlation analysis for evaluating the artificial", *Can. J. Civ. Eng.*, **31**(1), 56-64. https://doi.org/10.1139/l03-074.

Yuan, Y.C., Li, S.C., Li, L.P., Lei, T., Wang, S. and Sun, B.L. (2016), "Risk evaluation theory and method of collapse in mountain tunnel and its engineering applications", *J. Central South Univ.*, **47**(7), 2406-2414.

Zhang, G.H., Jiao, Y.Y., Chen, L.B., Wang, H. and Li, S.C. (2015), "Analytical model for assessing collapse risk during mountain tunnel construction", *Can. Geotech. J.*, **53**(2), 326-342. https://doi.org/10.1139/cgj-2015-0064.

Zhang, Y.Y., Jia, Y., Li, M. and Hou, L. (2018), "Spatiotemporal variations and relationship of PM and gaseous pollutants based on gray correlation analysis", *J. Environ. Sci. Health Part A-Tox/Hazard Subst. Environ. Eng.*, **53**(2), 139-145. https://doi.org/10.1080/10934529.2017.1383122.

Zhou, Z.Q., Li, S.C., Li, L.P., Shi, S.S. and Xu, Z.H. (2015), "An optimal classification method for risk assessment of water inrush in karst tunnels based on grey system theory", *Geomech. Eng.*, **8**(5), 631-647. https://doi.org/10.12989/gae.2015.8.5.631.

GC

List of abbreviation and symbols

X	Evaluation index sequence
Z	Reference sequence
Z_0	Normalized reference sequence
η	Resolution coefficient
P	The average of correlation coefficients sequence
E_k	The mean squared error of the neural network
θ_j	Threshold of the jth neuron in the output layer
w_{hj}	Connection weight of the hth and jth neurons
β_j	The input of the jth neuron in the output layer
b_h	The hth neuron output of the hidden layer
γ_h	The hth neuron threshold of the hidden layer
$g_h^{(m)}$	The threshold gradient of the m-layer
$b_h^{(m)}$	The hidden-layer neuron output of the m-layer
Z_i	Distribution density function of observation

μ_1	The expected value of j before the change point
μ_2	The expected value of j after the change point
σ_1^2	The variance in j before the change point
σ_2^2	The variance in j after the change point
A1	Longitudinal wave velocity
A2	Density
A3	Poisson's ratio
A4	Burial depth of tunnel
A5	Groundwater development
A6	Surrounding rock support type
A7	Support close time
A8	Construction management level
B1	Vault subsidence
B2	Horizontal convergence